Vortex noise and fluctuation conductivity in Josephson-junction arrays

Ing-Jye Hwang* and D. Stroud†
Department of Physics, The Ohio State University, Columbus, Ohio 43210
(Received 18 April 1997; revised manuscript received 14 October 1997)

We study the vortex number noise $S_v(\omega)$ and fluctuation conductivity $\sigma_1(\omega)$ in two-dimensional Josephson-junction arrays at three different applied magnetic fields, corresponding to zero, one-half, and $\frac{1}{24}$ of a flux quantum per plaquette ($f=0$, $\frac{1}{2}$ and $\frac{1}{24}$). S_v and σ_1 are obtained by numerically solving the equations for the coupled overdamped resistively-shunted-junction model with Langevin noise to simulate the effects of temperature. In all three cases, we find that $S_v(\omega)\propto\omega^{-3/2}$ at high frequencies ω and flattens out to become frequency independent at low ω, indicative of vortex diffusion, while $\sigma_1\sim\omega^{-2}$ at sufficiently high ω and $\sim\omega^0$ at low frequencies. Both quantities show clear evidence of critical slowing down and a simplified scaling behavior near the normal-to-superconducting transitions at $f=0$ and $f=\frac{1}{2}$, indicating that the vortex diffusion coefficient is approaching zero and the charge-carrier relaxation time is diverging at these temperatures. At $f=\frac{1}{24}$, there is no clear phase transition; instead, the vortex diffusion coefficient diminishes continuously as the temperature is lowered towards zero. The critical slowing down of $S_v(\omega)$, but not its frequency dependence, is in agreement with recent experiments on the flux noise $S_\Phi(\omega)$ in Josephson-junction arrays, which show a $1/\omega$ frequency dependence. We speculate about some possible reasons for the absence of a $1/\omega$ frequency regime. [S0163-1829(98)05110-8]

I. INTRODUCTION

Josephson-junction arrays (JJA's) and thin-film superconductors are excellent model systems for studying vortex dynamics. At zero magnetic field, such systems are believed to undergo a Kosterlitz-Thouless-Berezinskii[1,2] (KTB) transition at a temperature $T_{\rm KTB}$. At temperatures below $T_{\rm KTB}$ the vortices and anti-vortices are bound into pairs, whereas above $T_{\rm KTB}$ these pairs start to unbind into unpaired vortices. Such a phase transition is expected to affect a variety of transport properties of such systems.[3] Indeed, measurements of both the *I-V* characteristics and the inverse kinetic inductance consistent with the occurrence of a KTB transition have been reported in both thin superconducting films[4] and superconducting arrays.[5] When the applied field is a rational fraction f of flux quanta per plaquette, i.e., $f=p/q$, where p and q are small mutually prime integers, there is still thought to be a finite-temperature phase transition at a temperature $T_c(f)$,[6] but of a different character: below $T_c(f)$ there is a spatially ordered arrangement of vortices and antivortices, which becomes disordered at $T_c(f)$. At some fields, the phase transition may be accompanied, as at $f=0$, by the dissociation of thermally excited vortex-antivortex pairs.

The experimental study of vortex motion involves more than equilibrium properties. In transport measurements, the Magnus force generated by external currents causes the vortices to move and dissipate energy. But conventional transport measurements, such as *I-V* characteristics, measure the global response of all the vortices. If, on the other hand, one uses a superconducting quantum interference device (SQUID) placed over one portion of the Josephson-junction array, one can measure the *local* vortex response. One such response is the magnetic-flux noise generated by fluctuations in the local number of vortices within that area.

A number of groups have studied flux noise in superconductors. Several measurements have been carried out in high temperature superconducting films, including $Bi_2Sr_2CaCu_2O_{8+\delta}$ (Ref. 7) and $YBa_2Cu_3O_{6.95}$.[8] Recently, Shaw *et al.*[9] have done noise experiments on overdamped JJA's consisting of superconducting Nb islands in a Cu film, greatly extending some earlier measurements by Lerch *et al.*[10] These experiments yield a range of behavior for the spectral function $S_\Phi(\omega)$ of the flux noise, that is, the frequency Fourier transform of the flux-flux correlation function. For example, $YBa_2Cu_3O_{6.95}$ (Ref. 8) and JJA's (Ref. 9) are found to have $S_\Phi(\omega)\propto\omega^{-1}$ at ''high'' frequencies (''high,'' in this context, meaning greater than about 10–1000 Hz), while in $Bi_2Sr_2CaCu_2O_{8+\delta}$ (Ref. 7) $S_\Phi(\omega)\propto\omega^{-3/2}$ at similar frequencies.

There have also been several theoretical studies of flux noise in such systems. Houlrik *et al.*[11] discussed the behavior of flux noise from a Coulomb gas analogy, and calculated $S_\Phi(\omega)$ from a time-dependent Ginzburg-Landau model. At high frequencies, they found $S_\Phi(\omega)\propto\omega^{-2}$. Gronbech-Jensen *et al.*[12] studied a JJA with a static magnetic field of $\frac{1}{2}$ flux quantum per plaquette, using the so-called resistively shunted junction (RSJ) model including self-capacitance. Their primary interest, however, was to find the voltage noise at finite external currents, with disorder in the islands' positions, rather than the flux noise itself. Recently, Wagenblast and Fazio[13] have studied the flux noise and scaling behavior using an *XY* model with an assumed local damping for the phases, using a Coulomb gas analog. The local damping term corresponds to Ohmic resistance shunts coupling each superconducting grain to the ground. The resulting flux noise was found to be white for low frequencies, and to vary as ω^{-2} at high frequencies, and ω^{-1} at intermediate frequencies. Very recently, Tiesinga *et al.*[14] have used both the coupled RSJ model and an *XY* model with local damping to study flux noise numerically over a relatively limited frequency range. They concluded that their locally damped *XY* results did produce a $1/\omega$ flux noise with critical properties

near the KTB transition, and hence were closer to the experiment of Shaw *et al.*[9] than were the RSJ predictions.

In this paper, we carry out extensive calculations of flux noise in an array of coupled overdamped Josephson junctions, using Langevin noise to simulate the effects of temperature. Our model is similar to the RSJ model discussed by Tiesinga *et al.*,[14] but we study the real part of the frequency-dependent fluctuation conductivity $\sigma_1(\omega)$ in addition to the vortex noise, and we calculate both over a considerably wider frequency range. In addition we consider not only the unfrustrated case ($f=0$) but also the fully frustrated array ($f=\frac{1}{2}$) and the low-field case ($f=\frac{1}{24}$). As discussed further below, we do not calculate the flux noise directly; instead, we compute the *vortex number noise* $S_v(\omega)$ (defined below) which is presumed to be closely related to the actual measured quantity — the flux noise. In all three cases, our results for the vortex number noise show a clear signature of vortex diffusion above $T_{\rm KTB}$, i.e., $S_v(\omega)\propto\omega^{-3/2}$ above a cutoff frequency ω_v(T) which appears to approach zero near $T_c(f)$ for $f=0$ and $f=\frac{1}{2}$. For $f=\frac{1}{24}$, there is no clear phase transition and the cutoff frequency appears to diminish monotonically with decreasing temperature.

To calculate the fluctuation conductivity $\sigma_1(\omega)$, we make use of the well-known Kubo formalism, which connects $\sigma_1(\omega)$ to the Fourier transform of the current-current correlation function. The resulting $\sigma_1(\omega)$, like the vortex number noise, shows signs of critical slowing down near the phase transitions at $T_c(0)$ and $T_c(f=\frac{1}{2})$, and to diminish monotonically with temperature for $f=\frac{1}{24}$. But $\sigma_1(\omega)$ differs from $S_v(\omega)$ in that at high frequencies $\sigma(\omega)\sim\omega^{-2}$ rather than $\omega^{-3/2}$.

The remainder of this paper is organized as follows. Section II describes the formalism and numerical methods used to carry out these calculations. In Sec. III, we give our results for $f=0$, $f=\frac{1}{2}$, and $f=\frac{1}{24}$. Section IV discusses our results, primarily in terms of a possible scaling interpretation, and suggests some plausible extensions. Some brief concluding remarks follow in Sec. V.

II. FORMALISM

A. Model and method of solution

The details of the RSJ model can be found in the literature.[15] The current through a junction between two superconducting islands i and j is assumed to consist of three contributions in parallel: a normal current $I_{R;ij}=V_{ij}/R_{ij}$ through a resistance R_{ij}; a Josephson current $I_{S;ij}=I_{c;ij}\sin(\theta_{ij}^{\mathbf{A}})$; and a thermal noise current $I_{L;ij}$:

$$I_{ij}=\frac{V_{ij}}{R_{ij}}+I_{c;ij}\sin(\theta_{ij}^{\mathbf{A}})+I_{L:ij}\,. \tag{1}$$

Here $I_{c;ij}$ is the critical current,

$$\theta_{ij}^{\mathbf{A}}=\theta_i-\theta_j-A_{ij} \tag{2}$$

is the gauge-invariant phase difference across the junction, and is defined to lie in the range $(-\pi,\pi]$. $V_{ij}\equiv V_i-V_j$ is the voltage difference between islands i and j. The phase factor $A_{ij}=(2\pi/\Phi_0)\int_i^j\mathbf{A}\cdot d\mathbf{l}$, where $\mathbf{A}$ is the vector potential, and $\Phi_0=hc/2e$ is the flux quantum. In what follows, we will assume that $\mathbf{A}$ is due to the (time-independent) external magnetic field, and neglect any contributions to it from the induced fields. The voltage difference is related to the phases by the Josephson relation $V_{ij}=(\hbar/2e)d(\theta_{ij}^{\mathbf{A}})/dt$. Finally, $I_{L;ij}(t)$ is the Langevin noise current which simulates the effects of thermal noise between grains i and j; it is a Gaussian random variable characterized by the correlation functions

$$\langle I_{L;ij}(t)\rangle_e=0 \tag{3}$$

and

$$\langle I_{L;ij}(t)I_{L;kl}(t')\rangle_e=\frac{2k_BT}{R_{ij}}\delta(t-t')\,\delta_{ij;kl}\,, \tag{4}$$

where $\langle\cdots\rangle_e$ denotes an ensemble average.

Kirchhoff's law of current conservation implies that

$$I_{i;\rm ext}=\sum_{j\neq i}I_{ij}\,, \tag{5}$$

where $I_{i;\rm ext}$ is the external current fed into the ith grain. In the present work we consider only the case $I_{i;\rm ext}=0$. Equation (5) combined with the explicit expression Eq. (1) for I_{ij}, leads to the following set of coupled first-order nonlinear differential equations in the variables θ_i:

$$\sum_j\,(G_0)_{ij}\frac{\hbar}{2e}\dot{\theta}_j=D_i\,, \tag{6}$$

where $(G_0)_{ij}=-1/R_{ij}$ for $i\neq j$ and $(G_0)_{ii}=-\Sigma_{j\neq i}G_{ij}$. The inhomogeneous term is

$$D_i=I_{i;\rm ext}-\sum_{j\neq i}I_{c;ij}\sin(\theta_{ij}^{\mathbf{A}})-\sum_{j\neq i}I_{L;ij}\,. \tag{7}$$

We solve these coupled equations numerically by a standard algorithm for square lattices of several sizes, as discussed, for example, by Chung *et al.*[15] We assume no external current, and use periodic boundary conditions for an $N_s=N\times N$ square lattice of size with no disorder, i.e., $I_{c;ij}=I_c$ and $R_{ij}=R$ for all i,j, and either no external magnetic field ($f=0$) or a magnetic field of $\frac{1}{2}$ or $\frac{1}{24}$ of a flux quantum per plaquette ($f=\frac{1}{2}$ or $\frac{1}{24}$). The time iteration is accomplished using a second-order Runge-Kutta procedure with time intervals of order $dt=0.02\tau_0$, where $\tau_0=\hbar/(2eRI_c)$ is the characteristic time of the problem. The Langevin noise is treated according to the standard procedure described, for example, by Chung *et al.*[15]

B. Physical observables

If we solve these coupled equations including the assumed Langevin dynamics, we can calculate not only *time-dependent quantities*, but also various *equilibrium quantities*,[16] which are computed as time averages. We begin by describing the equilibrium quantities of interest here, then those which depend on time.

In the following, our results are presented in the ''natural units'' of the problem. Thus, the natural unit of time is $\tau_0=\hbar/(2eRI_c)$ and of frequency, $\omega_0=1/\tau_0$. Energy and temperature are given in units of $\hbar I_c/(2e)$.

Among the equilibrium quantities of interest are the helicity modulus tensor γ_{ij},[17] which measures stiffness against long-wavelength twists in the phase. For example, γ_{xx} is given by[18]

$$N_s\gamma_{xx}=\sum_{\langle ij\rangle} E_{J;ij}x_{ij}^2\langle\cos(\theta_{ij}^{\mathbf{A}})\rangle-\frac{1}{k_BT}(\langle E_x^2\rangle-\langle E_x\rangle^2), \quad (8)$$

where $x_{ij}=x_i-x_j$ and $E_x=\Sigma_{\langle ij\rangle}E_{J;ij}x_{ij}\sin(\theta_{ij}^{\mathbf{A}})$. To within a multiplicative constant, γ_{ij} is the superfluid density tensor of the array; for the present (two-dimensional square) array, it is a multiple of the unit tensor, and may be written $\gamma_{ij}=\gamma\delta_{ij}$ where δ_{ij} is the Kronecker delta.

It is also useful to define a *vortex number* $n(\mathbf{r})$ for each plaquette where $\mathbf{r}$ represents the center of plaquette. First we introduce the frustration f by $\Phi=(n+f)\Phi_0$, where n is an integer and Φ is the flux per plaquette due to the applied magnetic field (assumed uniform). Then $n(\mathbf{r})$ is an integer scalar defined by

$$n(\mathbf{r})=f+\frac{1}{2\pi}\sum_{\text{plaquette}}\theta_{ij}^{\mathbf{A}}. \quad (9)$$

The summation is taken around the plaquette boundary in the counterclockwise direction (viewed from the positive z axis). With this definition, the total algebraic number of vortices per plaquette, averaged over the entire lattice, will usually equal f. The value of $n(\mathbf{r})$ is $+1$ or -1 when there is one vortex or one antivortex within plaquette $\mathbf{r}$, and 0 when there is no vortex. We will assume periodic boundary conditions.

Given the above definition, we can introduce several derived quantities. For example, we can calculate

$$N_{v,\mathcal{A}}=\sum_{\mathbf{r}\in\mathcal{A}} n(\mathbf{r}), \quad (10)$$

where the sum runs over all plaquettes within some area $\mathcal{A}$ of the array. Similarly, the density of vortex-antivortex pairs is sometimes of interest; it is defined by

$$\Delta n_z=\frac{1}{N_{\mathcal{A}}}\sum_{\mathbf{r}\in\mathcal{A}} n(\mathbf{r})^2-f, \quad (11)$$

where $N_{\mathcal{A}}$ represents the number of plaquettes in $\mathcal{A}$. In the definition of Eq. (11), we choose $N_{\mathcal{A}}=N_s$. By subtracting f, we remove the field-induced vortices, so that Δn_z represents the number of thermally excited vortex-antivortex pairs. Also of interest is the density-density correlation function

$$g(\mathbf{r})=\frac{1}{N_sf^2}\sum_{\mathbf{r}'}\langle n(\mathbf{r}')n(\mathbf{r}'+\mathbf{r})\rangle. \quad (12)$$

The corresponding Fourier transform is the vortex structure factor

$$S(\mathbf{k})=\frac{1}{N_s}\sum_{\mathbf{r}} g(\mathbf{r})\exp(i\mathbf{k}\cdot\mathbf{r}). \quad (13)$$

Next, we turn to the dynamical observables. Many of these are spectral functions, that is, the Fourier transforms of time-correlation functions. For example, the real part of the xx component of the fluctuation conductivity tensor $\sigma_{1,xx}(\omega)$ may be expressed as such a correlation function, using the Kubo formula.[19] In the classical limit ($\hbar\omega\ll k_BT$), this theorem gives

$$\sigma_{1,xx}(\omega)=\frac{1}{N_sk_BT}\int_0^\infty dt\cos(\omega t)\langle J_x(t)J_x(0)\rangle. \quad (14)$$

Here

$$J_x=\frac{1}{a^2}\sum_{\langle ij\rangle} I_c\sin(\theta_{ij}^{\mathbf{A}}) \quad (15)$$

is the x component of the supercurrent density; the sum runs over all bonds in the x direction and a is the lattice constant. In the present isotropic case, $\sigma_{1,ij}$ is diagonal with $\sigma_{1,ij}(\omega,T)\equiv\sigma_1(\omega,T)\delta_{ij}$. The integral of expression (14) over all frequencies gives the *integrated fluctuation conductivity*

$$\gamma_2\equiv\frac{1}{\pi}\int_0^\infty\sigma_1(\omega)d\omega=\frac{1}{N_sk_BT}\langle|J_x(t=0)|^2\rangle. \quad (16)$$

The vortex number noise $S_{v;\mathcal{A}}(\omega)$ is defined as

$$S_{v,\mathcal{A}}(\omega)=\frac{1}{N_s}\times\lim_{T_0\to\infty}\frac{1}{T_0}\left\langle\left|\int_{-T_0/2}^{+T_0/2}N_{v,\mathcal{A}}(t)\exp(-i\omega t)dt\right|^2\right\rangle, \quad (17)$$

where T_0 is the integration time, usually taken as around $5-8\times10^3\tau_0$. The quantity of greatest experimental interest is not the vortex number noise, of course, but rather the flux noise itself, $S_{\Phi,\mathcal{A}}(\omega)$. In the present work, we will simply assume that these two quantities behave similarly. In actuality, the flux noise should be calculated directly from the flux-flux time-correlation function. In principle, this should in turn be computed directly from the fluctuation currents, using Maxwell's equations; it will depend not only on the vortex number but also on various geometry-specific quantities, such as the height above the array where the SQUID is placed. Such a calculation, though more difficult, should nonetheless be carried out in order to get the most realistic estimates of $S_\Phi(\omega)$.

III. RESULTS

A. $f=0$

At $f=0$, the overdamped Josephson array should exhibit a KTB transition at a temperature $T_{\text{KTB}}\equiv T_c(f=0)\sim0.90\hbar I_c/(2ek_B)$.[20] Below that temperature, the thermally excited vortices and antivortices form into bound pairs, which start to dissociate above T_{KTB}. This is reflected in the behavior of the time-averaged mean-square vortex density Δn_z [Eq. (11)] shown in Fig. 1. Specifically, Δn_z becomes nonzero near T_{KTB}, where the vortex-antivortex pairs begin to unbind. This is expected, because, above T_{KTB}, the existence of unbound pairs means that the number of vortices and antivortices within $\mathcal{A}$ is more likely to fluctuate away from zero. Although Δn_z is not expected to vanish sharply at T_{KTB}, nonetheless T_{KTB}, as estimated from

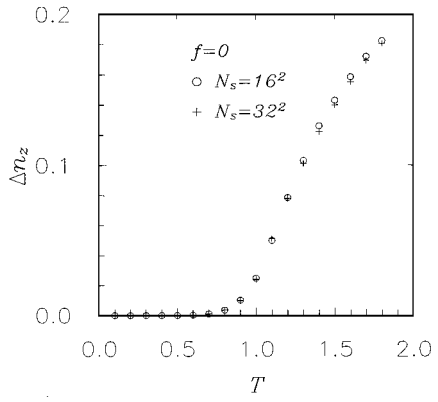

FIG. 1. Time-averaged mean-square vortex density Δn_z for the overdamped array at zero magnetic field ($f=0$), plotted as a function of temperature T for two different array sizes.

the vanishing of $\Delta N_{v,\mathcal{A}}$, is close to its accepted value of $0.90\hbar I_c/(2ek_B)$ for an infinite lattice.[20]

Figure 2 shows the helicity modulus γ, as well as the integral of the fluctuation conductivity, $\gamma_2=(1/\pi)\int_{-\infty}^{\infty}\sigma_1(\omega)d\omega$. γ and γ_2 are calculated from Eqs. (8) and (16).[18] Both are obtained as appropriate time averages of the RSJ solutions with Langevin noise. $\gamma(T)$ shows a characteristic jump from zero to a finite value at $T_{\rm KTB}$; the expected universal jump, of magnitude $(2/\pi)T_{\rm KTB}$, is somewhat broadened in our calculations by finite-size effects. γ_2 shows a characteristic peak near $T_{\rm KTB}$ where γ itself goes to zero. In general, the peak in γ_2 is less sharp than that found in Ref. 18 for the 3D case. We attribute the difference primarily to our use of a temperature-independent critical current I_c. In a real Josephson array, I_c is strongly temperature dependent; this will greatly reduce the peak in γ_2 for $T>T_{\rm KTB}$, leading to a much sharper peak.

Next, we turn to the vortex number noise $S_{v,\mathcal{A}}(\omega)$, as defined in Eq. (17). We must be careful in calculating this quantity with periodic boundary conditions, because $N_{v,\mathcal{A}}$ would be identically zero if $\mathcal{A}$ were the entire array area. For a smaller $\mathcal{A}$, N_v does fluctuate in time, giving rise to vortex

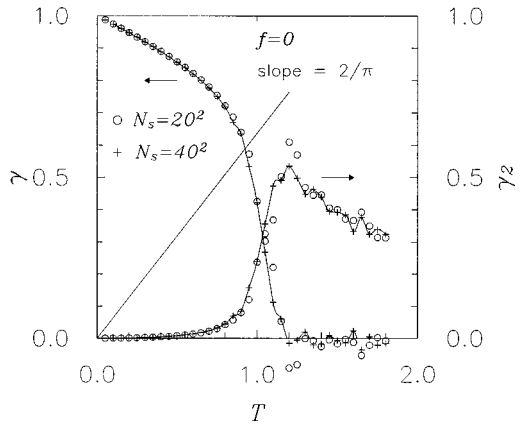

FIG. 2. Helicity modulus γ [Eq. (8)] and integrated fluctuation conductivity γ_2 [Eq. (16)] for an overdamped array at zero magnetic field and two different array sizes, as calculated from time-averaged solutions to RSJ equations with Langevin noise.

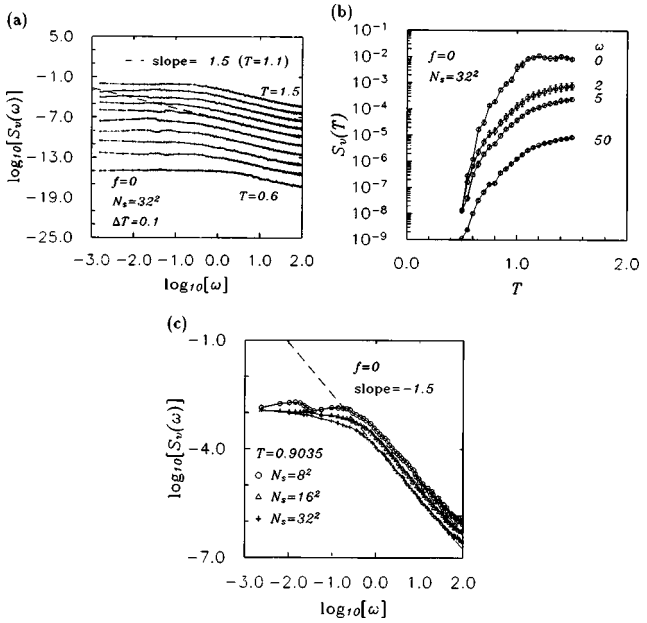

FIG. 3. Vortex number noise $S_{v,\mathcal{A}}(\omega)$ [Eq. (17)] at zero applied magnetic field ($f=0$), plotted (a) versus frequency ω for several temperatures T; (b) versus temperature at several ω; and (c) versus different N_s at fixed temperature. All quantities are plotted in natural units, as described in the text, and in all cases, $\mathcal{A}$ is one-fourth the area of the array. The curves in (a) are vertically displaced; the dashed lines have slope $-3/2$.

number noise. Our results for $S_{v,\mathcal{A}}$ are shown as a function of frequency for several temperatures in Fig. 3(a) for a square area $\mathcal{A}\equiv\ell^2$ equal to 1/4 of the array area. Note that the curves have been vertically displaced for clarity. The same results are shown in Fig. 3(b), for different frequencies as a function of T. Finally, Fig. 3(c) shows these results for different sizes at fixed temperature.

All these curves show certain similarities. At low frequencies, $S_{v,\mathcal{A}}$ becomes roughly frequency independent, but at high frequencies $S_v(\omega)\sim\omega^{-3/2}$, a dependence which is known to characterize diffusive behavior.[21] The spectral function thus clearly shows the characteristic signature of vortex diffusion at temperatures above $T_{\rm KTB}$.

The frequency $\omega_v(T)$ characterizing the crossover between frequency independent and $\omega^{-3/2}$ behavior is plotted in the inset of Fig. 4. It gives strong indications of *critical slowing down*. That is, $\omega_v(T)$ seems to approach zero as T approaches $T_{\rm KTB}$ from either side. This behavior can be interpreted in terms of the vortex diffusion coefficient, using the approximate relation[21] $D\approx\ell^2\omega_v$ which connects the D to the vortex noise spectrum in a fixed area ℓ^2. This relation combined with the apparent critical slowing down suggests that the effective vortex diffusion coefficient $D\to 0$ as $T\to T_{\rm KTB}$.

The plots for $S_{v,\mathcal{A}}(\omega)$ for different temperatures can all be collapsed onto a single curve of $S_{v,\mathcal{A}}(\omega,T)/S_{v,\mathcal{A}}(0,T)$ with respect to ω/ω_v as shown in the main part of Fig. 4. This is further striking evidence of critical slowing down near a continuous phase transition, and is discussed further in the next section.

Figure 5(a) shows $\sigma_1(\omega,T)$, as calculated directly from the fluctuation-dissipation theorem, Eq. (14),[19] for several

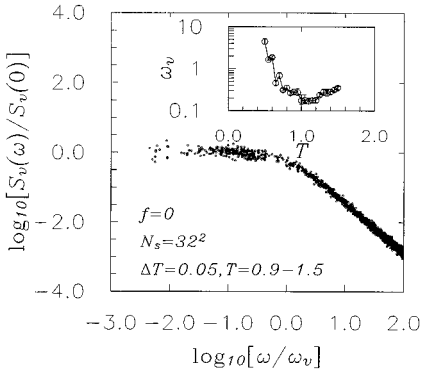

FIG. 4. $S_{v,\mathcal{A}}(\omega,T)/S_{v,\mathcal{A}}(0,T)$ versus ω/ω_v for $f=0$, where $\omega_v(T)$ is the crossover frequency. Inset: Crossover frequency $\omega_v(T)$ between frequency-independent and $\omega^{-3/2}$ behavior in $S_{v,\mathcal{A}}(\omega,T)$.

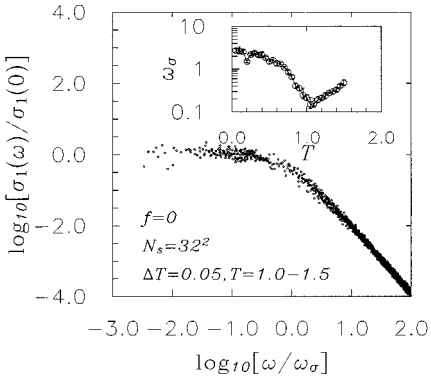

FIG. 6. $\sigma_1(\omega,T)/\sigma_1(0,T)$ plotted as a function of $\omega/\omega_\sigma(T)$ for $f=0$. Inset: Crossover frequency $\omega_\sigma(T)$ between frequency-independent and ω^{-2} behavior in $\sigma_1(\omega,T)$.

different temperatures at $f=0$. For a fixed temperature, $\sigma_1(\omega)$ flattens out at low frequencies and falls off at high frequencies approximately as ω^{-2}. The slight upward convexity at high frequency here (and for the noise calculation described above) is an artifact of the fast-Fourier transform used to evaluate these quantities. Figure 5(b) shows $\sigma_1(\omega,T)$ at several fixed ω's. At the lowest frequency (nominally $\omega=0$, but actually an average over several $\omega<0.08$), there is a strong peak at $T\approx T_{\rm KTB}$. For the other frequencies (all greater than ω_0), no peak is discernable near $T_{\rm KTB}$, indicating that the influence of the transition is suppressed at such high frequencies. By comparing these results with those of Fig. 2, we see that the peak in γ_2 is dominated by the *low-frequency* regime of $\sigma_1(\omega)$, i.e., $\omega<\omega_0$. Finally, Fig. 5(c) shows $\sigma_1(\omega,T)$ plotted as a function of ω at a fixed temperature and several lattice sizes N_s.

Figure 6 shows $\sigma_1(\omega,T)/\sigma_1(0,T)$ plotted as a function of $\omega/\omega_\sigma(T)$, where $\omega_\sigma(T)$ is the crossover frequency between

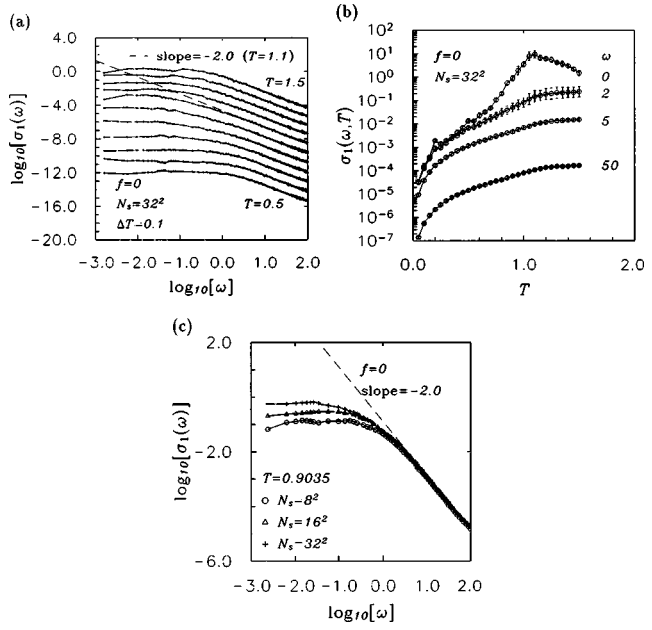

FIG. 5. (a)–(c). Same as Figs. 3(a)–3(c), but for $\sigma_1(\omega)$. Dashed lines in (a) and (c) have slopes -2.

ω^0 and ω^{-2} behavior. Like the results for $S_{v;\mathcal{A}}$ in Fig. 4, the data collapse shown here is further evidence of critical slowing down near $T_{\rm KTB}$. The crossover between the two limits occurs at a frequency $\omega_\sigma(T)$ shown in the inset of Fig. 6 which, like $\omega_v(T)$ is *strikingly temperature-dependent*, approaching zero near $T=T_{\rm KTB}$.

B. $f=\frac{1}{2}$

At $f=\frac{1}{2}$, a square Josephson junction array is believed to undergo a continuous phase transition at a temperature $T_c(f=\frac{1}{2})\sim 0.45\hbar I_c/2e$.[22] Below this transition, the array is characterized by a checkerboard arrangement of vortices and antivortices, while above it, the vortices are distributed with no long-range order.[22] The disordering which occurs at $T_c(f=\frac{1}{2})$ is simultaneously accompanied by dissociation of thermally excited vortex-antivortex pairs. This dissociation is similar to that which occurs at the KTB transition at $f=0$, but in contrast to that transition, it is characterized by an apparently *nonuniversal* jump in the helicity modulus $\gamma(T)$.

We have evaluated both $\gamma(T)$ and the structure factor $S(\mathbf{Q})$ for $\mathbf{Q}=(\pi/a,\pi/a)$ as a function of temperature, by solving the Langevin equations of motion. As expected, $S(\mathbf{Q})$ (Fig. 7) vanishes fairly smoothly near $T=T_c(f=\frac{1}{2})$, while $\gamma(T)$ (Fig. 8) falls continuously to zero near that temperature, suggestive of a continuous phase transition. The integrated fluctuation conductivity $\gamma_2(T)$, also shown in Fig. 8, shows a noticeable peak near $T_c(f=\frac{1}{2})$, as at $f=0$. Also at that temperature, the quantity Δn_z (Fig. 7) behaves in a manner suggesting a vortex-antivortex unbinding transition. All these phenomena occur near the same temperature, suggesting that there is only a single phase transition. While this behavior has long been known from Monte Carlo studies, the present work shows that the same single transition also manifests itself in dynamical simulations.

Another aspect of vortex lattice melting can be observed in Fig. 9. This figure shows that the Bragg peak in the structure factor changes from a δ-function character for $T<T_c(f=\frac{1}{2})$ to a broad, liquidlike peak for $T>T_c(\frac{1}{2})$.

The phase transition is once again reflected in the vortex number noise $S_{v,\mathcal{A}}(\omega)$ (Fig. 10). For all temperatures, $S_{v;\mathcal{A}}\sim\omega^{-3/2}$ at high frequencies and flattens out to vary as ω^0 at low frequencies. The crossover between the two behaviors

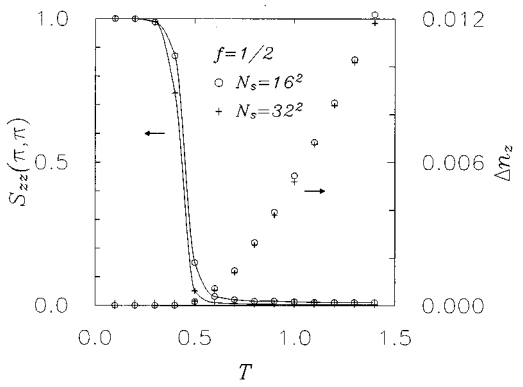

FIG. 7. Left scale: structure factor $S(\mathbf{Q},T)$ versus T for $\mathbf{Q}=(\pi/a,\pi/a)$ at $f=\frac{1}{2}$. Right scale: Time-averaged mean-square vortex density Δn_z as a function of temperature for $f=\frac{1}{2}$.

occurs at a frequency $\omega_v(T)$ which once again vanishes as $T\rightarrow T_c(f=\frac{1}{2})$ from either side. This critical slowing is suggested in Fig. 10(a) and is made even clearer in the inset of Fig. 11, where we plot the crossover frequency as a function of temperature. The main part of Fig. 11 shows, as at $f=0$, that the noise curves for different temperatures can be collapsed into a single plot of $S_{v,\mathcal{A}}(\omega,T)$ as a function of $\omega/\omega_v(T)$. This collapse is suggestive of scaling behavior which is discussed further below.

The real part of the fluctuation conductivity $\sigma_1(\omega)$ [Figs. 12(a) and 12(b)] also reflects both the phase transition and the critical slowing down. As at $f=0$, $\sigma_1(\omega,T)$ is roughly frequency independent at low frequencies, and falls off as ω^{-2} at high frequencies, consistent with Drude behavior. The crossover from low-frequency to high-frequency behavior occurs at a frequency $\omega_\sigma(T)$ which approaches zero as $T\rightarrow T_c(\frac{1}{2})$ from either side (cf. inset of Fig. 13), and the conductivity curves for different temperatures can be collapsed onto a single plot as does the vortex noise (main part of Fig. 13).

C. $f=\frac{1}{24}$

At small values of f, the behavior of an overdamped array is expected to differ from that at $f=0$ and $f=\frac{1}{2}$. At these

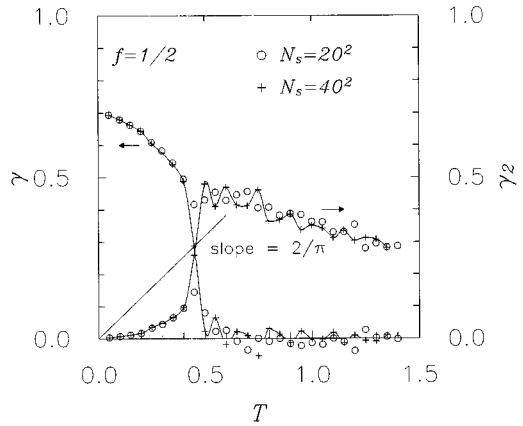

FIG. 8. Helicity modulus $\gamma(T)$ and integrated fluctuation conductivity $\gamma_2(T)$ for $f=\frac{1}{2}$.

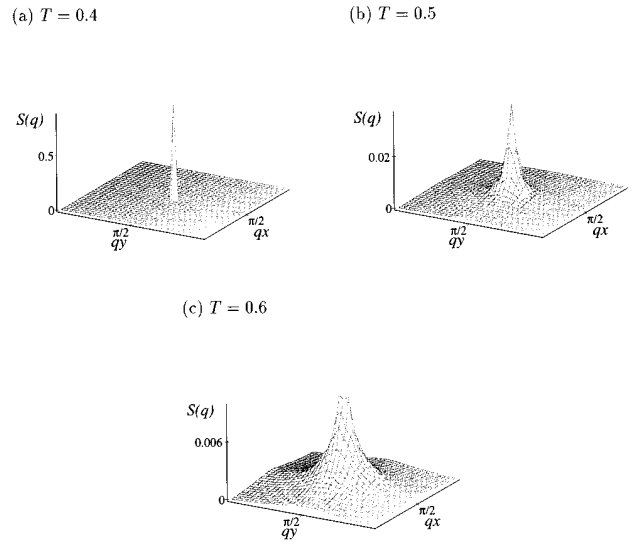

FIG. 9. Perspective plot of the vortex-vortex structure factor $S(\mathbf{q})$ for $f=\frac{1}{2}$ at several temperatures above and below the superconducting-normal phase transition near $T_c(f=\frac{1}{2})=0.45J/k_B$, as a function of $\mathbf{q}=(q_x,q_y)$ in a 32×32 array.

small values, the density of field-induced vortices is quite low, suggesting that any freezing of these vortices into an ordered configuration will occur at a much lower temperature than at $f=\frac{1}{2}$.[22] At temperatures well above this low-f freezing, one expects the field-induced vortices to form a liquidlike state with no long-range order. The flux noise should reflect this structure, or lack of it: one might expect behavior characteristic of independent diffusion by individual vortices.

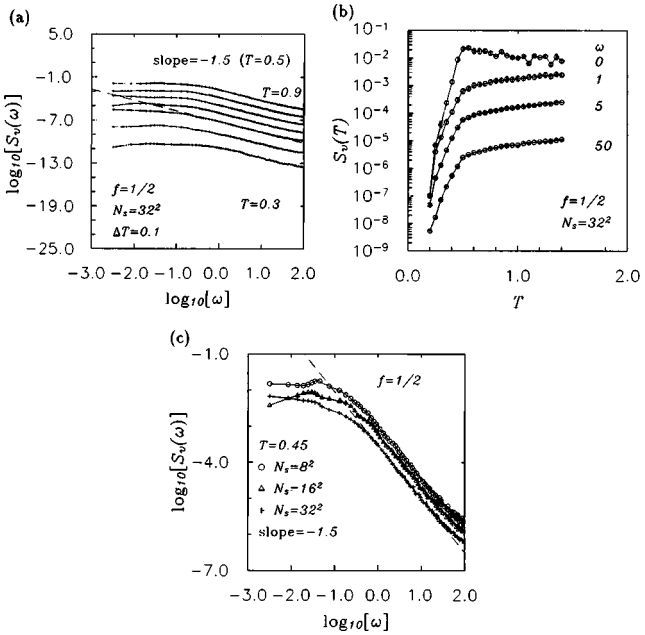

FIG. 10. (a) Vortex number noise $S_{v,\mathcal{A}}(\omega,T)$, plotted as a function of ω for various temperatures T at $f=\frac{1}{2}$. Curves are vertically displaced for clarity. (b) Same as (a) but plotted versus temperature for fixed ω and *not* displaced vertically; (c) versus different N_s at fixed temperature. Dashed lines have slope $-3/2$.

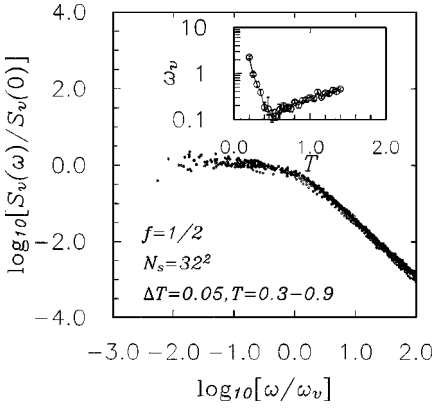

FIG. 11. Scaling plot of $S_{v,\mathcal{A}}(\omega,T)/S_{v,\mathcal{A}}(0,T)$ versus $\omega/\omega_v(T)$, where $\omega_v(T)$ is a crossover frequency between frequency-independent and $\omega^{-3/2}$ behavior. Inset: ω_v as a function of temperature.

In order to check this picture, we have calculated both $S_{v,\mathcal{A}}(\omega,T)$ and $\sigma_1(\omega,T)$ for a representative small field: $f=\frac{1}{24}$. The calculated vortex number noise and conductivities are plotted in Figs. 14 through 17 for a 24×24 array, which therefore contains 24 field-induced vortices.

The behavior differs strikingly in several ways from the other two fields. $S_{v,\mathcal{A}}$ still shows clear evidence of diffusive behavior, varying as ω^0 at low frequencies and $\omega^{-3/2}$ at high frequencies, and the plots for different temperatures still collapse as at $f=0$ and $f=\frac{1}{2}$. The diffusion coefficient D inferred from these plots, however, does not show obvious critical slowing down at any finite temperature. Instead, it seems to decrease monotonically with temperature. We have attempted to fit this behavior to various analytical forms, such as exponentially activated, but without success: the activation energy so obtained is temperature dependent.

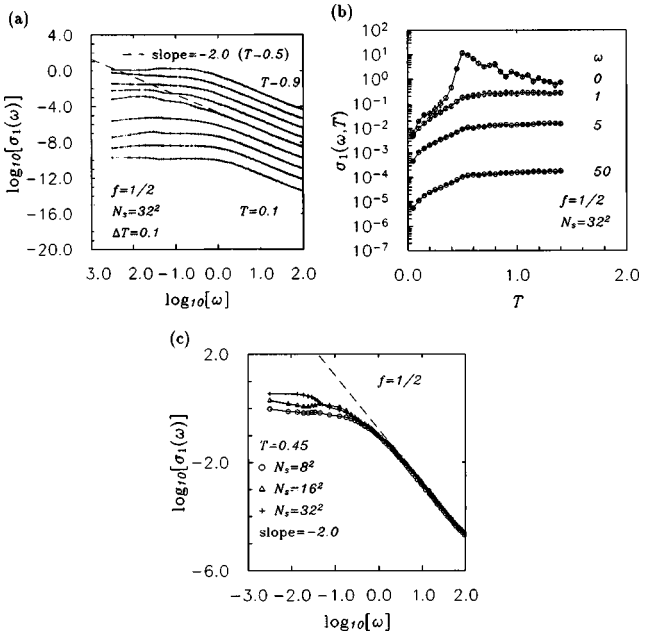

FIG. 12. Fluctuation conductivity $\sigma_1(\omega,T)$ for $f=\frac{1}{2}$ plotted (a) versus frequency ω for various T and (b) versus T for several ω; (c) versus T. Curves in (a) are vertically displaced for clarity. Dashed lines have slope -2.

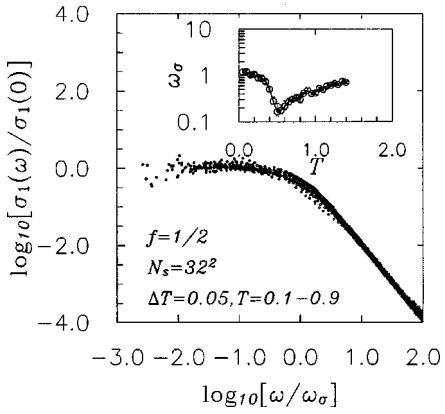

FIG. 13. Scaling plot of $\sigma_1(\omega,T)/\sigma_1(0,T)$ versus $\omega/\omega_\sigma(T)$, where $\omega_\sigma(T)$ (inset) is the crossover frequency between ω^0 and ω^{-2} behavior.

The fluctuation conductivity $\sigma_1(\omega)$ shows even more striking behavior. It still has the Drude form, and exhibits the same data collapse as at the other fields, but the crossover frequency ω_σ, while monotonically decreasing with decreasing temperature, seems to show a plateau near $T=0.7\hbar I_c/2e$. We believe that this is a residue of the zero-field XY transition near these temperatures, but broadened by the finite magnetic field. Likewise, we speculate that the minimum in $\sigma_1(\omega,T)$ itself near $k_BT=0.9\hbar I_c/2e$ is also related to the zero-field transition.

IV. DISCUSSION

A. Possibility of scaling for $f=0$ and $f=\frac{1}{2}$

We now discuss our numerical results for $f=0$ and $f=\frac{1}{2}$ in terms of a possible scaling interpretation. In the case of vortex number noise, a natural starting point is the scaling hypothesis suggested by Shaw *et al.*[9] for the vortex density-density correlation function:

$$\langle\rho_v(\mathbf{x},t)\rho_v(\mathbf{y},t')\rangle=\xi^{-s}F_1\left(\frac{t-t'}{\tau},\frac{|\mathbf{x}-\mathbf{y}|}{\xi},\frac{L}{\xi}\right). \quad (18)$$

Here $\tau(\sim1/\omega_v)$ is a characteristic time, which diverges near $T_c(f)$, and Shaw *et al.* suggest that $s=4$. In terms of this correlation function, the vortex number noise $S_{v;\mathcal{A}}(\omega)$ can also be expressed as a scaling function which, after some algebra, takes the form

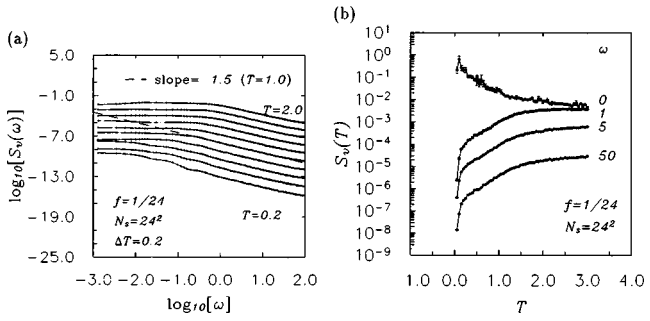

FIG. 14. Same as Fig. 10 but for $f=\frac{1}{24}$.

$$S_{v,\mathcal{A}}(\omega)=\frac{\tau}{L^2}\xi^{4-s}\tilde{F}\left(\omega\tau,\frac{L}{\xi},\frac{T_0}{\tau}\right), \tag{19}$$

where $\tilde{F}$ is another scaling function. According to a standard dynamical scaling assumption,[23] we expect that $\tau\sim\xi^z$ near T_c, where z is a dynamical critical exponent.

We now discuss how well these assumptions agree with our numerical results. If we assume that the integration time $T_0\gg\tau$, the last argument of $\tilde{F}$ is very large and can be ignored. Precisely at $T=T_c$, we can replace ξ by L. With these two assumptions, $\tilde{F}$ can be rewritten in terms of a single argument and

$$S_{v,\mathcal{A}}(\omega)\sim L^{2+z-s}G(\omega L^z), \tag{20}$$

where G is another scaling function. The predictions of this equation can be compared to the results of Figs. 3(c) and 10(c). Both figures suggest that $S_{v,\mathcal{A}}(\omega=0)$ is roughly size independent for large L. This implies that $z\sim s-2$ or $z=2$ assuming $s=4$, in agreement with the experimental estimate of Shaw *et al.* However, using $G(x)\sim x^{-3/2}$ at large ω, we obtain $S_{v;A}(\omega)\sim L^{2-s-(1/2)z}\omega^{-3/2}$, where $2-s-\frac{1}{2}z\sim-3$ using $s=4$, $z=2$. This is a much stronger size dependence than is seen in our numerical results.

The same scaling hypothesis leads to the prediction that the crossover frequency $\omega_v\sim\xi^{-z}$ for temperatures near $T_c(f)$. For $f=0$, we expect $\xi\sim\exp(b/\sqrt{T-T_c(0)})$, where b is a constant. While the universality class of the transition at $f=\frac{1}{2}$ remains a matter of debate,[24] it is likely that ξ will have a power-law dependence, $\xi(T)\sim|T-T_c(f)|^{-\nu}$, and hence that $\omega_v\sim|T-T_c(\frac{1}{2})|^{\nu z}$, near $T_c(\frac{1}{2})$. We have not obtained a good fit of our numerical data to these forms for either $f=0$ or $f=\frac{1}{2}$, possibly because the data is not sufficient to definitively prove or disprove the expected scaling form. In a finite area $\mathcal{A}$, the scaling form suggests that ω_v will never become smaller than a size-dependent value L^{-z}, which should be observed at $T_c(f)$. Once again, our numerical data is not sufficient to provide a definitive test for this prediction, though the data clearly suggests, for any size considered, that ω_v never vanishes, even at $T=T_c(f)$. This qualitative result would be in agreement with the scaling hypothesis.

It seems reasonable to describe the conductivity $\sigma_1(\omega,T,L)$ using a similar scaling approach. The proper scaling function should take the form

$$\sigma_1(\omega,T,L)=\xi^a S\left(\omega\tau,\frac{L}{\xi}\right), \tag{21}$$

where a is a suitable exponent and S a scaling function to be determined. Once again, we expect $\tau\sim\xi^{z'}$, where z' is a critical exponent possibly differing from z. At $T=T_c(f)$, we must replace ξ by L, and the above equation can be rewritten as

$$\sigma_1(\omega,T_c,L)=L^a\tilde{S}(\omega L^{z'}), \tag{22}$$

where $\tilde{S}$ is another scaling function.

At large x, our numerical data indicate that $\tilde{S}(x)\sim x^{-2}$, and also that $\sigma_1(\omega,T_c,L)$ is independent of L. These two conditions together imply that $a=2z'$, for both $f=0$ and $f=\frac{1}{2}$. In the limit $\omega\to0$, our data suggests that $\sigma_1(\omega,T_c,L)$ varies with L, roughly as $L^{1.5}$ but with considerable uncertainty, so that $a\sim1.5$ and $z'\sim0.75$. For $T\neq T_c(f)$, we have not succeeded in fitting $\omega_\sigma\equiv1/\tau$ to the expected scaling form $\omega_\sigma\sim\xi^{-z'}$, possibly because of insufficient numerical data.

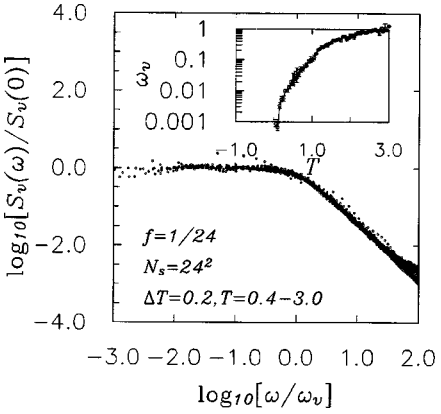

FIG. 15. Same as Fig. 11 but for $f=\frac{1}{24}$.

Figures 4, 6, 11, and 13 do suggest that our numerical data obey a kind of scaling. For example, in each case, as noted earlier, all the data for a given size collapse onto a single plot of $S_{v,\mathcal{A}}(\omega)/S_{v,\mathcal{A}}(0)$ versus ω/ω_v, or of $\sigma_1(\omega)/\sigma_1(0)$ versus ω/ω_σ. But we have not succeeded in obtaining a further collapse of the data onto the more specific scaling forms described in this section. It is possible that a better collapse might be obtained with larger-scale numerical simulations.

B. $f=\frac{1}{24}$

At $f=\frac{1}{24}$, our numerical results show no clear indication of a phase transition at finite temperatures; instead they are consistent with vortices whose diffusion coefficient is continuously diminishing as T decreases. This behavior agrees with other numerical studies which suggest that the vortex freezing temperature for small f is well below $0.1\hbar I_c/2e$.[25] For independent vortices, one might expect an exponentially activated diffusion coefficient, $D\propto\exp(-E_a/k_BT)$ with E_a a suitable activation energy, presumably that required to excite a vortex between one plaquette and an adjacent one.[26] While we have not been able to obtain a good fit to this form, the diffusion coefficient is certainly decreasing rapidly at low T. Similarly, the characteristic frequency for the conductivity, ω_σ, is decreasing quickly at low T, indicating that the relaxation time for scattering charge carriers is growing at low temperatures.

Our results for $\sigma_1(\omega,T)$ for this field show some structure near the zero-field transition temperature $T_c(f=0)$. Most notably, $\omega_\sigma(T)$ shows a pronounced inflection point near this temperature. We believe that at these low fields, $\omega_\sigma(T)$ is largely determined by T_{KTB} for $T>T_{\mathrm{KTB}}$, but for lower temperatures, ω_σ is sensitive to the finite density of field-induced vortices and decreases more slowly towards zero than at high temperatures.

C. Absence of $1/\omega$ flux noise

Our results differ from the $1/\omega$ behavior seen experimentally for $S_\Phi(\omega)$ in overdamped Josephson arrays[9] over sev-

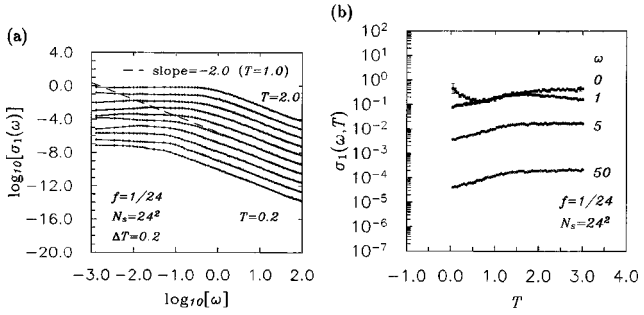

FIG. 16. Same as Fig. 12, but for $f=\frac{1}{24}$.

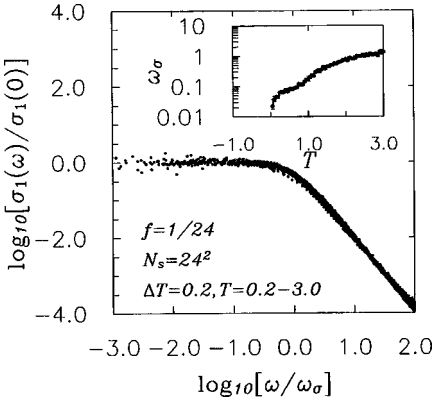

FIG. 17. Same as Fig. 13, but for $f=\frac{1}{24}$.

eral decades of frequency, although we do see indications of similar scaling behavior. In this subsection, we suggest several possible reasons why this observed behavior is absent from our calculations.

One possibility is that we are not using the most applicable dynamical equations for the array. Tiesinga *et al.* have already pointed out that a model incorporating local, rather than RSJ dynamics can produce a $1/\omega$ vortex number noise over a limited frequency range. In the present context, such a local dynamics would correspond to having each grain resistively shunted to the same ground, with no shunt resistances between the grains. One difficulty with such a local dynamics, when applied to an array of Josephson junctions, is that it does not produce the giant, and fractional giant Shapiro steps which are observed in arrays of overdamped Josephson junctions,[27] and which are correctly predicted by the coupled RSJ model.[28] A possible way out of this difficulty would be to include *both* sources of damping, i.e., both shunt resistances between grains and (much larger) resistive shunts R_g to a ground plane. This could conceivably be a reasonable model for the actual experimental geometry, and would probably (for large enough R_g) produce the observed Shapiro steps. We have not, however, carried out a numerical test of the noise produced by this model.

Another possible explanation is that the observed $1/\omega$ noise actually originates from properties of the individual junctions. It is well established that some Josephson tunnel junctions exhibit low-frequency $1/\omega$ voltage noise in the presence of an applied current above the critical current.[29] This noise is attributed to thermal fluctuations in the junction critical current I_c, which arise from the temperature dependence of I_c. Such critical current fluctuations are not included in our model; if they were, they would undoubtedly lead to similar, possibly $1/\omega$, fluctuations in the flux through a portion of the array. We believe that such I_c fluctuations to be a very plausible source of the observed $1/\omega$ flux noise, because they occur at the very low frequencies (1–1000 Hz) where the $1/\omega$ flux noise is actually observed. By contrast, the characteristic frequency of the vortex fluctuations calculated here, and in the local damping models, is $2eRI_c/\hbar \sim 1$ MHz. Even taking into account the critical slowing down we observe in our model, it seems that the dynamics may be too fast to be appropriate for the 1–1000 Hz regime.

Finally, we note again that we are computing the vortex number noise, rather than the flux noise itself. While the two undoubtedly differ, it seems unlikely that the difference could lead to a $1/\omega$ behavior of S_Φ which is absent from S_v. Thus, of the three explanations suggested here, we feel that the second of these (intrinsic $1/\omega$ noise in the individual junctions) is the most plausible.

In passing, we note again that measurements in $YBa_2Cu_3O_{6.95}$,[8] have also shown a similar $1/\omega$ frequency regime, but studies of very thin films of $Bi_2Sr_2CaCu_2O_{8+\delta}$ (Ref. 7) show a $1/\omega^{3/2}$ behavior similar to that found here, but in the 100 Hz–10 KHz frequency regime; this behavior is also interpreted as evidence for vortex diffusion. Our results show clear evidence of such diffusive behavior in a numerical model for the dynamics of a Josephson array; the diffusing objects in our calculations, as presumably in the $Bi_2Sr_2CaCu_2O_{8+\delta}$ films, are the thermally excited vortices and antivortices, and the field-induced vortices. The frequencies where we find diffusive behavior appear, however, to lie well above the diffusive regime in $Bi_2Sr_2CaCu_2O_{8+\delta}$.[7]

V. CONCLUSIONS

In conclusion, we have calculated both the vortex number noise $S_v(\omega)$ and the frequency-dependent conductivity $\sigma_1(\omega)$ in an overdamped Josephson-junction array at three different applied magnetic fields corresponding to 0, $\frac{1}{2}$, and $\frac{1}{24}$ of a flux quantum per plaquette. In all three cases, $S_v(\omega)$ shows a clear $\omega^{-3/2}$ behavior, characteristic of vortex diffusion, at high frequencies, and is frequency independent at low frequencies. The latter has a Drude behavior, varying as $1/\omega^2$ at high frequencies and ω^0 at low frequencies. Both quantities show clear evidence of critical slowing down (i.e., a vortex diffusion coefficient which goes to zero, and a charge-carrier relaxation time which diverges) near the superconducting transitions at $f=0$ and $f=\frac{1}{2}$, and there is some evidence of scaling behavior in both quantities. The absence of a clear $1/\omega$ regime is somewhat surprising; we have suggested several possible explanations, but a decisive explanation for this dependence remains to be determined.

ACKNOWLEDGMENTS

We are very grateful for the assistance and advice of Dr. Seungoh Ryu during the early stages of this work. Valuable conversations with Professor T. R. Lemberger are very much appreciated. This work was supported by NSF Grant No. DMR94-02131. This computation was carried out on SP2 of the Ohio Supercomputer Center.

*Electronic address: hwang@pacific.mps.ohio-state.edu
†Electronic address: stroud@ohstpy.mps.ohio-state.edu

[1] J. M. Kosterlitz and D. J. Thouless, J. Phys. C **6**, 1181 (1973).
[2] V. L. Berezinskii, Zh. Éksp. Teor. Fiz. **59**, 207 (1970) [Sov. Phys. JETP **32**, 493 (1971)].
[3] V. Ambegaokar *et al.*, Phys. Rev. B **21**, 1806 (1980); S. Doniach and B. A. Huberman, Phys. Rev. Lett. **42**, 1169 (1979); P. Minnhagen, Rev. Mod. Phys. **59**, 1001 (1987).
[4] M. R. Beasley *et al.*, Phys. Rev. Lett. **42**, 1165 (1979); A. F. Hebard and A. T. Fiory, *ibid.* **44**, 291 (1980).
[5] D. J. Resnick *et al.*, Phys. Rev. Lett. **47**, 1542 (1981); D. W. Abraham *et al.*, Phys. Rev. **26**, 5268 (1982); R. F. Voss and R. A. Webb, Phys. Rev. B **25**, 3446 (1982).
[6] W. Y. Shih, C. Ebner, and D. Stroud, Phys. Rev. B **30**, 134 (1984).
[7] C. T. Rogers *et al.*, Phys. Rev. Lett. **69**, 160 (1992).
[8] M. J. Ferrari *et al.*, Phys. Rev. Lett. **67**, 1346 (1991).
[9] T. J. Shaw *et al.*, Phys. Rev. Lett. **76**, 2551 (1996).
[10] Ph. Lerch *et al.*, Helv. Phys. Acta **65**, 389 (1992).
[11] J. Houlrik *et al.*, Phys. Rev. B **50**, 3953 (1994).
[12] N. Grønbech-Jensen *et al.*, Phys. Rev. B **46**, 11 149 (1992).
[13] K.-H. Wagenblast and R. Fazio, cond-mat/9611177 (unpublished).
[14] P. H. E. Tiesinga *et al.*, Phys. Rev. Lett. **78**, 519 (1997).
[15] See, e.g., S. R. Shenoy, J. Phys. C **18**, 5163 (1985); K. K. Mon and S. Teitel, Phys. Rev. Lett. **62**, 673 (1989); J. S. Chung *et al.*, Phys. Rev. B **40**, 6570 (1989); D. Domínguez and J. V. José, Int. J. Mod. Phys. B **8**, 3749 (1994).
[16] See, e.g., G. Parisi, *Statistical Field Theory* (Addison-Wesley, New York, 1988), Chap. 19.
[17] M. E. Fisher, M. N. Barber, and D. Jasnow, Phys. Rev. A **8**, 1111 (1973).
[18] C. Ebner and D. Stroud, Phys. Rev. B **28**, 5053 (1983).
[19] See, e.g., R. K. Pathria, *Statistical Mechanics* (Butterworth, Oxford, 1995), p. 477; or L. D. Landau and E. M. Lifshitz, *Statistical Physics: Part I* (Pergamon, New York, 1980), Chap. 12.
[20] G. Ramirez-Santiago and J. V. José, Phys. Rev. Lett. **68**, 1224 (1992); Phys. Rev. B **49**, 9567 (1994).
[21] R. F. Voss and J. Clarke, Phys. Rev. B **13**, 556 (1976).
[22] S. Teitel and C. Jayaprakash, Phys. Rev. B **27**, 598 (1983).
[23] See, for example, B. I. Halperin and P. Hohenberg, Rev. Mod. Phys. **49**, 435 (1977).
[24] See, for example, C. Denniston and C. Tang, Phys. Rev. Lett. **79**, 451 (1997).
[25] S. Teitel and C. Jayaprakash, Phys. Rev. Lett. **51**, 1999 (1983).
[26] C. J. Lobb, D. W. Abraham, and M. Tinkham, Phys. Rev. B **27**, 150 (1983).
[27] S. Benz, M. Rzchowski, M. Tinkham, and C. J. Lobb, Phys. Rev. Lett. **64**, 693 (1990).
[28] K. H. Lee and D. Stroud, Phys. Rev. B **43**, 5280 (1991).
[29] J. Clarke and G. Hawkins, Phys. Rev. B **14**, 2826 (1976).